NAVAL POSTGRADUATE SCHOOL

MONTEREY, CALIFORNIA

THESIS

STATISTICAL ANALYSIS OF ACOUSTIC SIGNAL PROPAGATING THROUGH THE SOUTH CHINA SEA BASIN

by

Meihuei Chen

March 2016

Thesis Advisor:	Ching-Sang Chiu
Co-Advisor:	Christopher W. Miller

Approved for public release; distribution is unlimited

THIS PAGE INTENTIONALLY LEFT BLANK

REPORT DOCUMENTATION PAGE			*Form Approved OMB No. 0704–0188*
Public reporting burden for this collection of information is estimated to average 1 hour per response, including the time for reviewing instruction, searching existing data sources, gathering and maintaining the data needed, and completing and reviewing the collection of information. Send comments regarding this burden estimate or any other aspect of this collection of information, including suggestions for reducing this burden, to Washington headquarters Services, Directorate for Information Operations and Reports, 1215 Jefferson Davis Highway, Suite 1204, Arlington, VA 22202-4302, and to the Office of Management and Budget, Paperwork Reduction Project (0704-0188) Washington, DC 20503.			
1. AGENCY USE ONLY ***(Leave blank)***	**2. REPORT DATE** March 2016	**3. REPORT TYPE AND DATES COVERED** Master's thesis	
4. TITLE AND SUBTITLE STATISTICAL ANALYSIS OF ACOUSTIC SIGNAL PROPAGATING THROUGH THE SOUTH CHINA SEA BASIN			**5. FUNDING NUMBERS**
6. AUTHOR(S) Meihuei Chen			
7. PERFORMING ORGANIZATION NAME(S) AND ADDRESS(ES) Naval Postgraduate School Monterey, CA 93943-5000			**8. PERFORMING ORGANIZATION REPORT NUMBER**
9. SPONSORING /MONITORING AGENCY NAME(S) AND ADDRESS(ES) N/A			**10. SPONSORING / MONITORING AGENCY REPORT NUMBER**
11. SUPPLEMENTARY NOTES The views expressed in this thesis are those of the author and do not reflect the official policy or position of the Department of Defense or the U.S. Government. IRB Protocol number ____N/A____.			
12a. DISTRIBUTION / AVAILABILITY STATEMENT Approved for public release; distribution is unlimited			**12b. DISTRIBUTION CODE**

13. ABSTRACT (maximum 200 words)

During the Windy Islands Soliton Experiment, two deep water moorings were deployed 167 km apart in the northeastern South China Sea (SCS) basin to study the effects of nonlinear internal waves on 400-Hz acoustic signal propagation. The acoustic arrival structure for this path shows five significant arrivals, exhibiting multi-scale variability in travel time and intensity. Time series of moored temperature data, travel time of the first and a late arrival, as well as measured sound intensity were constructed. By analyzing the power spectral density of those time series, six internal tidal constituents were identified, with strong diurnal and semidiurnal energy. The variances in the temperature and travel time were dominated by the internal tides, while the largest variance in signal intensity was in the high-frequency internal-wave band. Coherence analysis of the temperature and travel times indicated that the travel time variance in the tidal band was more related to the temperature fluctuation in the west of the SCS basin. The observed standard deviations of signal intensity level were plotted against the number of independent arrivals, showing that the relation converges to a modified statistical theory of phase-random multipaths.

14. SUBJECT TERMS nonlinear internal waves, acoustics, South China Sea, statistics, sound propagation variability			**15. NUMBER OF PAGES** 43
			16. PRICE CODE
17. SECURITY CLASSIFICATION OF REPORT Unclassified	**18. SECURITY CLASSIFICATION OF THIS PAGE** Unclassified	**19. SECURITY CLASSIFICATION OF ABSTRACT** Unclassified	**20. LIMITATION OF ABSTRACT** UU

NSN 7540–01-280-5500

Standard Form 298 (Rev. 2–89)
Prescribed by ANSI Std. 239–18

THIS PAGE INTENTIONALLY LEFT BLANK

Approved for public release; distribution is unlimited

STATISTICAL ANALYSIS OF ACOUSTIC SIGNAL PROPAGATING THROUGH THE SOUTH CHINA SEA BASIN

Meihuei Chen
Lieutenant, Taiwan Navy
B.S., Chinese Naval Academy, 2007

Submitted in partial fulfillment of the
requirements for the degree of

MASTER OF SCIENCE IN PHYSICAL OCEANOGRAPHY

from the

NAVAL POSTGRADUATE SCHOOL
March 2016

Approved by: Ching-Sang Chiu
Thesis Advisor

Christopher W. Miller
Co-Advisor

Peter Chu
Chair, Department of Oceanography

THIS PAGE INTENTIONALLY LEFT BLANK

ABSTRACT

During the Windy Islands Soliton Experiment, two deep water moorings were deployed 167 km apart in the northeastern South China Sea (SCS) basin to study the effects of nonlinear internal waves on 400-Hz acoustic signal propagation. The acoustic arrival structure for this path shows five significant arrivals, exhibiting multi-scale variability in travel time and intensity. Time series of moored temperature data, travel time of the first and a late arrival, as well as measured sound intensity were constructed. By analyzing the power spectral density of those time series, six internal tidal constituents were identified, with strong diurnal and semidiurnal energy. The variances in the temperature and travel time were dominated by the internal tides, while the largest variance in signal intensity was in the high-frequency internal-wave band. Coherence analysis of the temperature and travel times indicated that the travel time variance in the tidal band was more related to the temperature fluctuation in the west of the SCS basin. The observed standard deviations of signal intensity level were plotted against the number of independent arrivals, showing that the relation converges to a modified statistical theory of phase-random multipaths.

THIS PAGE INTENTIONALLY LEFT BLANK

TABLE OF CONTENTS

THIS PAGE INTENTIONALLY LEFT BLANK

LIST OF FIGURES

LIST OF ACRONYMS AND ABBREVIATIONS

BW	bandwidth
cpd	cycles per day
CSD	cross-spectrum density
D	diurnal
DOF	degree of freedom
HIW	high-frequency internal wave
IT	internal tide
NIW	nonlinear internal wave
PSD	power spectral density
RR	refracted-refracted
SCS	South China Sea
SD	semi-diurnal
SIL	sound intensity level
SPL	sound pressure level
SRBR	surface-reflected bottom-reflected

THIS PAGE INTENTIONALLY LEFT BLANK

ACKNOWLEDGMENTS

I would like to express my deepest gratitude to Professors Ching-Sang Chiu and Christopher W. Miller. Without your guidance and patience, I would not have been able to complete this thesis.

The preparation and deployment of the instruments and moorings were well-conducted by the researchers and students of the Naval Postgraduate School and National Taiwan University. Without their skills and expertise, this work would not have been possible.

The Windy Island Soliton Experiment was sponsored by the National Science Council (NSC, Taiwan), Taiwan Ministry of Science and Technology (MOST, Taiwan) and the Office of Naval Research (ONR, USA).

THIS PAGE INTENTIONALLY LEFT BLANK

I. INTRODUCTION

The northern part of the South China Sea (SCS) is a basin surrounded by the Luzon Strait at its east and the continental shelf at its west. The Kuroshio current flows westward from the Pacific Ocean, through the Luzon Strait to the basin. This current interacts with two ridges at the Luzon Strait bottom and generates some of the largest nonlinear internal waves (NIWs) in the world. Their amplitudes were found to be greater than 100 m, with propagation speeds more than 3 m/s (Ramp et al. 2004). These strong waves transport energy, cause a mixing of the water column, and induce large variability of the ocean environmental profiles such as temperature and salinity. The variability of environmental conditions can affect underwater sound propagation.

Since the northern SCS is an important region for antisubmarine warfare, the understanding of underwater acoustic signal behavior is crucial for the naval planning and tactical deployments. The Windy Island Soliton Experiment (WISE) was designed to study the characteristics of these energetic NIWs and their influence on acoustic signal transmission.

A. WISE BASIN EXPERIMENT

The Windy Island Soliton Experiment was a collaboration between researchers at the Naval Postgraduate School, National Taiwan University, and the National Sun Yat-Sen University, whose focus was to characterize the properties of trans-basin NIWs and their effects on acoustic signal propagation in the northern SCS.

During the WISE basin experiment, two moored arrays instrumented with temperature and pressure sensors, a sound source and a receiver, were placed in approximate alignment with the internal waves' propagation direction, between the Luzon Strait and the Chinese continental slope (Figure 1). The acoustic source at the B2 (East) mooring transmitted a phase-modulated signal with a carrier frequency of 400 Hz and bandwidth of 80 Hz every 15 minutes. Processing the signal received at the B1 mooring (West) yields the arrival structure of a pulse, whose change in travel time and sound intensity over the eight-month period can be monitored (Bernotavicius et al. 2010).

The focus of this thesis will be on the data collected from June to October 2006, during which large-scale variability was observed.

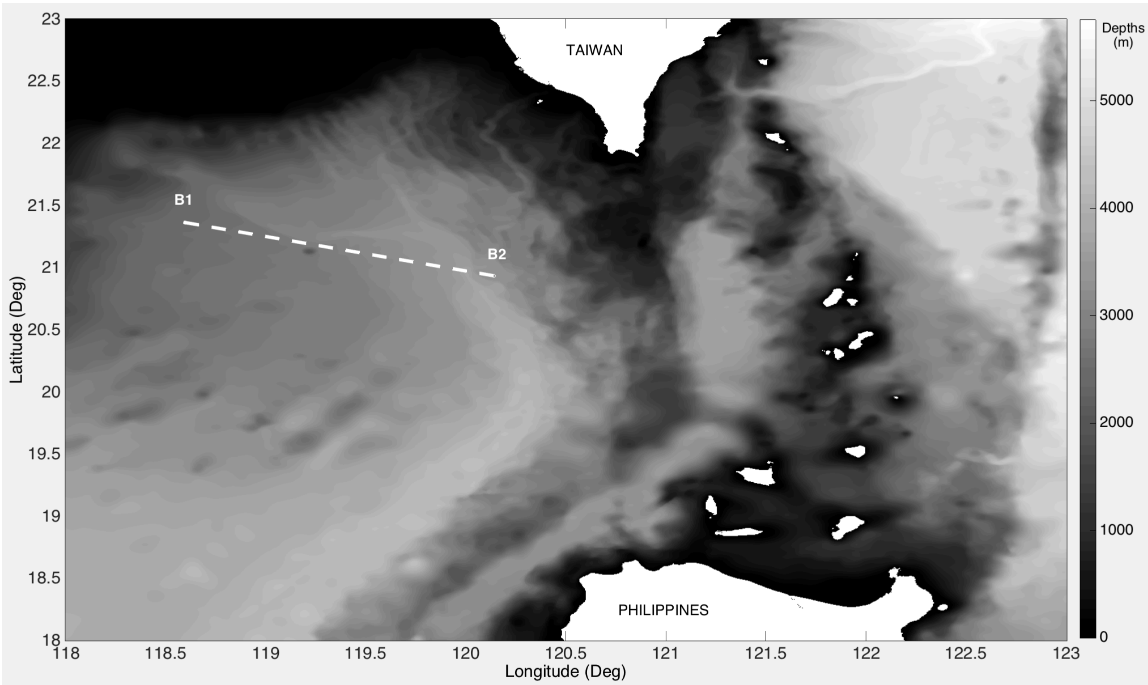

Figure 1. Locations of the source (B2) and receiver (B1) in the South China Sea during the WISE deep basin experiment. The moorings are 167 km apart, south of Taiwan, located between the Luzon Strait and the Chinese continental slope, in ~3000m water depth (from Bernotavicius et al. 2010).

B. OBJECTIVES

There are two objectives of this thesis. The first is to study the impact of the trans-basin NIWs on a low-frequency acoustic signal propagating through a long distance within the SCS basin via statistical methods. The second, to investigate the application of a modified statistical theory regarding sound intensity level fluctuation in deep water transmissions. Previously, this modified theory was successfully tested with shallow-water transmission data (Reeves, 2008).

C. APPROACH

To study the temporal fluctuations observed in the received WISE acoustic data, time series analysis techniques were applied to temperature, acoustic travel time, and intensity data sets. First, the spectra of each data series was estimated to examine the distribution of variance in various frequency bands, then the coherence of time series pairs were calculated to study their linear relationship. Lastly, the acoustic signals were filtered and the intensity statistics, as a function of bandwidth, were evaluated to investigate the applicability of a modified theory of sound intensity as a function of independent arrivals.

D. THESIS OUTLINE

This thesis comprises four chapters. Chapter II describes the time series used in this thesis, the statistical tools applied during analysis and their reliability estimates. Chapter III presents the results of the time series analyses and provides a discussion of the NIWs' properties and their influence on acoustic signal transmission. The thesis concludes with a summary in Chapter IV.

THIS PAGE INTENTIONALLY LEFT BLANK

II. DATA AND METHODS

This chapter includes the origins of the data and the approaches used to examine the data. The raw temperature and sound pressure data were collected during the WISE deep basin experiment and manipulated into five time series. Time series tools such as power spectral density estimation and the coherence were used to analyze each data set and combination of data sets, to identify and characterize the observed trends and variation, and the underlying physical phenomenon that cause these effects. The criteria required to evaluate sound intensity level (SIL) as a function of independent arrivals, is presented in the last section of this chapter.

A. DATA

Two moorings were deployed in the east and west of the SCS basin during the WISE deep-water experiment. A sound source was placed on the east mooring at a depth of 840 m, and a hydrophone receiver was located on the west mooring at the same depth. Temperature sensors collected data from each mooring at a depth of ~840 m (Figure 2). These temperatures show obvious long- and short-term periodic patterns. The acoustic source transmitted a 400 Hz phase-modulated signal, with a bandwidth of 80 Hz and source level (SL) of 183 dB re 1μPa, every 15 minutes. The received signal was processed via matched-filtering to produce a multipath arrival structure showing five significant arrivals for each transmission (Figure 3). Multi-scale temporal fluctuations of the travel time and the received sound pressure level were seen in the received arrival structures over the course of the experiment. The first arrival shows a prominent large scale fluctuation spanning weeks/months, in addition to the short-term, higher frequency fluctuations. The later arrivals also show the short-term variability in travel time, but the longer scale fluctuations of the early arrival are not visually apparent.

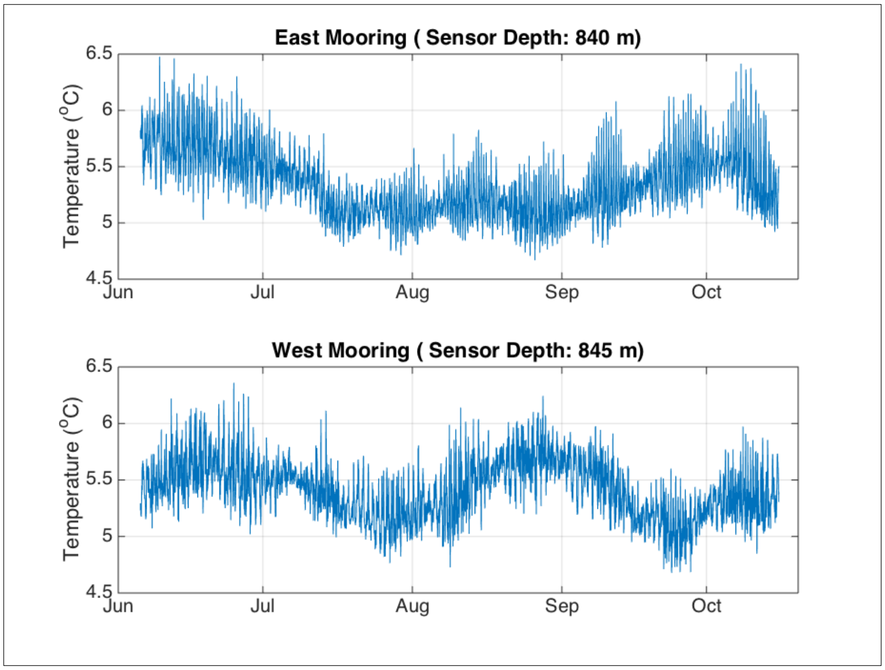

Figure 2. Observed temperature time series at the east (top) and west (bottom) moorings. Long- and short-term variability are seen.

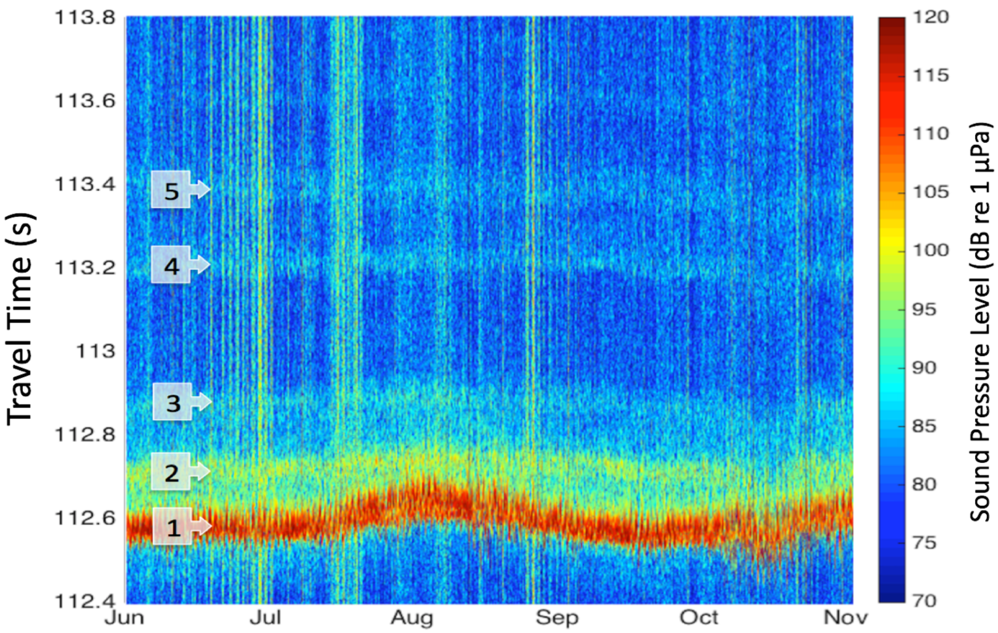

Figure 3. The arrival structure of the received signals as a function of transmission time. Five significant arrivals and multiscale variability in travel time and pressure level are seen.

Bernotavicius et al. (2010) modeled the 400 Hz signal transmission path of the WISE deep basin experiment. The modeled single transmission arrival structure showed five arrivals, with a multipath time spread consistent with the observed data (Figure 4, top). The modeled ray paths of the first arrival group were refracted-refracted (RR) rays (Figure 4, panel 2). The remaining, later arrivals were surface-reflected bottom-reflected (SRBR) rays, which spanned the entire water column and interacted with the sea surface and bottom, causing additional bottom losses along these paths (Figure 4, panel 3–6 panel).

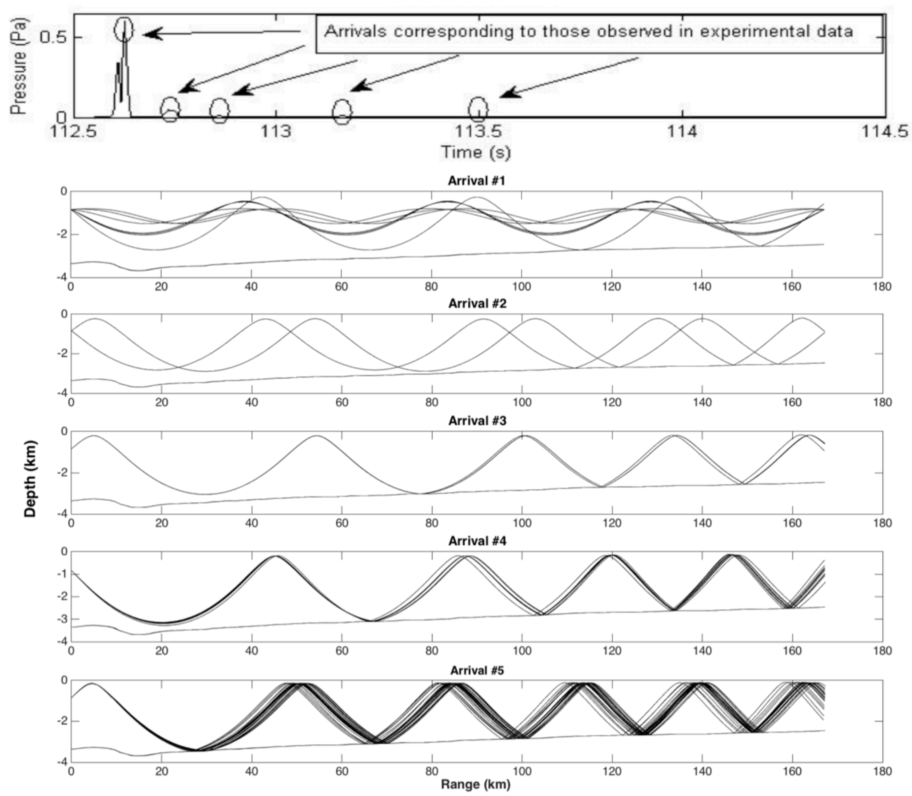

Figure 4. Bernotavicius et al. (2010) modeling results of the 400 Hz acoustic signal from the WISE experiment. The modeled arrival structure (top panel) shows five arrivals. The ray paths for each arrival (panels 2 through 6) show that except for the 1st arrival traveling through the refracted-refracted path, the later arrivals interact with the surface or bottom.

The travel times of the first and fourth arrivals were extracted to be used in a detailed time-series analysis in this thesis (Figure 5, top & middle). A time series of the sound pressure level (SPL) was also constructed (Figure 5, bottom), by integrating the square of the processed pressure signal in the time domain over the multipath spread, and averaging over the preprocessed length of the signal, for an analysis of signal intensity fluctuation. Note that the pulse compression processing used a signal energy conserving matched filter.

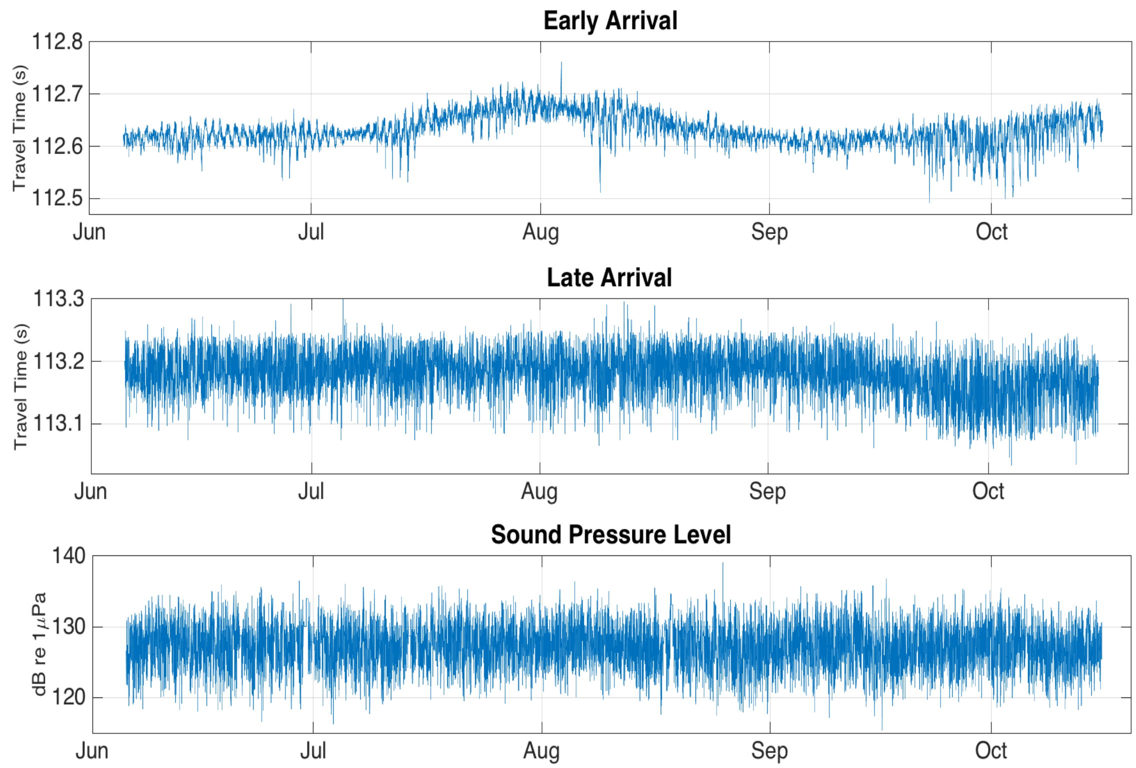

Figure 5. The travel-time time series of the 1st arrival (top, "early" arrival) and the 4th arrival (middle, "late" arrival) were constructed. The early arrival travel time shows clear multi-scale variability, while in the late arrival time series, longer scale variability was not clear. The SPL time series is in the bottom panel.

B. METHODS OF ANALYSIS

The fluctuation of the temperature, travel time, and SPL data series are associated with ocean wave processes of various wavelengths. Analyzing the data as a function of frequency rather than time is needed to identify effects of ocean wave fluctuations observed in each time series, their statistical properties, and relationships. Spectral decomposition was used on each time series to view each spectrum. The coherence of two variables was used to further analyze the linear dependence between variable pairs.

Following the methods of Reeves (2008), the SIL fluctuations were evaluated as a function of independent arrivals, by applying two rules to classify what constitutes a significant, independent arrival. The statistical relation was tested against a modified theory of Dyer (1970).

1. Power Spectrum Density

For a stochastic stationary process, the power spectral density (PSD) of a time series reveals the frequency distribution of a signal's variance. It can be estimated from an ensemble of the Fourier transforms of independent segments of a time series, or equivalently by a running average (i.e., frequency smoothing) of the square of the Fourier transform of the entire time series (Emery and Thompson 2004). Using the frequency smoothing technique, the single-sided estimate of the PSD, given a time series x(t), is

$$\hat{G}_{xx}(f,B) = \frac{2}{T_r B}\int_{f-B/2}^{f+B/2} \left|X(f')\right|^2 df'$$

where B is the width of the frequency smoothing window, X is the Fourier transform of the time series, with record length T_r.

For a time series with normal statistics, this PSD estimate is a random variable with a chi-square distribution with $2T_rB$ degrees of freedom (DOF). Because the estimated PSD distribution is known, the reliability of the estimates can be evaluated by calculating the confidence intervals. The true value of the single-sided PSD at given frequency is expected to fall into the interval

$$\frac{v\hat{G}_{xx}(f)}{\chi^2_{v,\,\alpha/2}} \le G_{xx}(f) \le \frac{v\hat{G}_{xx}(f)}{\chi^2_{v,\,1\text{-}\alpha/2}},\ v = 2BT_r$$

at the (1-α)100 % confidence (Emery and Thompson 2004).

In this research, three bandwidths were utilized during the frequency smoothing process to ensure the reliability of the spectra in the meso-, tidal and internal wave scale frequencies. Smoothing bands of 0.1, 0.2, and 1 cycle per day (cpd), respectively, were used over the spectral frequency ranges 0 to 2.5 cpd, 2.5 to 6.5 cpd, and 6.5 to the end of the spectrum. The 95% CIs were also calculated for each of the averaging bands to quantify the estimates.

2. Squared Coherence

The PSD describes the frequency characteristics of a single time series, while the squared coherence spectrum measures the linear dependence between two time series. The squared coherence is a function of the PSDs of each time series and their cross-spectral density (CSD). The CSD can be estimated via the same frequency smoothing process used to estimate the PSD. Given the spectra of the time series x(t) and y(t), the estimated squared coherence function is given by

$$\hat{\gamma}^2_{xy}(f) = \frac{\left|\hat{G}_{xy}(f)\right|^2}{\hat{G}_{xx}(f)\hat{G}_{yy}(f)}$$

where G_{xy} is the estimated CSD.

To quantify the reliability of the estimates, Thompson (1979) developed an equation that expresses the squared coherence of totally uncorrelated x and y can occur by chance up to

$$\gamma^2_{1-\beta} = 1 - \beta^{1/(BT_r - 1)},$$

at the confidence level (1-β)100%. The value $\gamma^2_{1-\beta}$ is known as the pure chance limit, and is determined by the selection of the frequency smoothing band, B, and ensemble length, T_r, used in CSD calculation. When the estimated squared coherence exceeds the pure chance limit, a linear dependence exists between the two time series at the corresponding frequency.

3. Independent Arrival Criteria

Dyer (1970) proposed that the random fluctuations of noise intensity depend on the number of independent sources. If each source has a different frequency and propagates via independent groups of multipaths, then the received mean-square pressure from this source signal has a chi-square distribution with two DOF. For each additional independent source, the number of DOF will increase by two, and the variance of the received mean square pressure will decrease. The acoustic signals transmitted during the WISE deep-basin experiment arrived at the receiver after propagating along independent multipaths. The independent arrivals in the arrival structure may be viewed as statistically similar to Dyer's "independent source." Therefore, it was hypothesized that the received sound intensity fluctuation can be related to the number of independent arrivals (Reeves 2008). Reeves successfully tested this hypothesis (the modified Dyer's theory) against a shallow water transmission data set. The final piece of this thesis research is to test this modified Dyer's theory against deep-water transmission data.

Low-pass filtering the received acoustic signal at different cutoff frequencies varies the number of arrivals with respect to the signal bandwidth (Figure 6), consistent with the inverse relation of signal bandwidth and pulse width. Narrowband signals have broader pulse width, causing neighboring arrivals to "merge," appearing as one broad arrival. Broadband signals have narrower pulse width resulting in an increase in resolvable arrivals. For our statistical analysis, an arrival has to be composed of a ray or a group of rays that propagating through independent paths, and not overlapping in the time with its adjacent arrivals. Therefore, two criteria were made in this study to determine the independence of the arrivals.

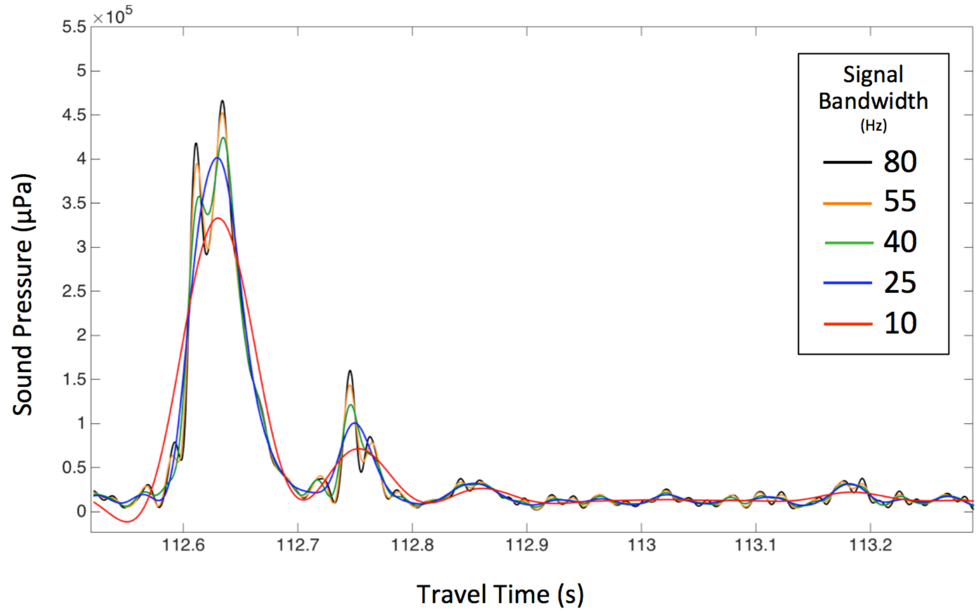

Figure 6. An example transmission, showing the full-band (black) signal and the various low-passed filtered signals (color) used to calculate the number of arrivals versus bandwidth. As the signal bandwidth is reduced, it is clearly evident that pulse resolution is lowered, causing a reduction in the number of arrivals.

For the first criteria, an arrival had to be "significant," or have sufficient magnitude to be counted as an arrival, rather than random noise. This was accomplished using a dynamic noise threshold to ensure arrivals had significant received amplitude. For each arrival structure reception (Figure 7), the received signal (blue) had a multipath spread of 1.5s, so the analyzed noise level (red) was also calculated using a 1.5s-long segment of noise much later in the arrival structure. A threshold was then applied at twice the maximum noise level, that is +6 dB above the maximum noise level, to identify the signal arrivals (peaks) that have significant receive levels. Since the noise level fluctuated in each transmission, the establishment of this threshold ensured that the selected arrivals were the products of the transmitted signal, rather than random fluctuations in the noise.

After identifying the significant arrivals, the next criterion was to examine their independence with adjacent arrivals. After examining a number of individual arrivals, it was determined that this transmission path has negligible sound-channel dispersion. This allows the measurement of the half-amplitude pulse width, inversely proportional to the signal bandwidth. A computer simulation study of this signal consistently found that the half-amplitude pulse width,

$$\tau = \frac{1.3}{BW}$$

where *BW* is the bandwidth of the processed pulse. To guarantee the independence of the significant arrivals, we require that the minimum temporal separation of adjacent arrivals be greater than 2τ.

For example, Figure 7 shows a transmission with five significant arrivals, and their temporal width (distance between black dotted lines) are measured. The separation between the 2nd and 3rd arrival is less than the minimum temporal separation (red double arrow), thus they are considered as an independent arrival group. In this case, the total number of independent arrivals is four.

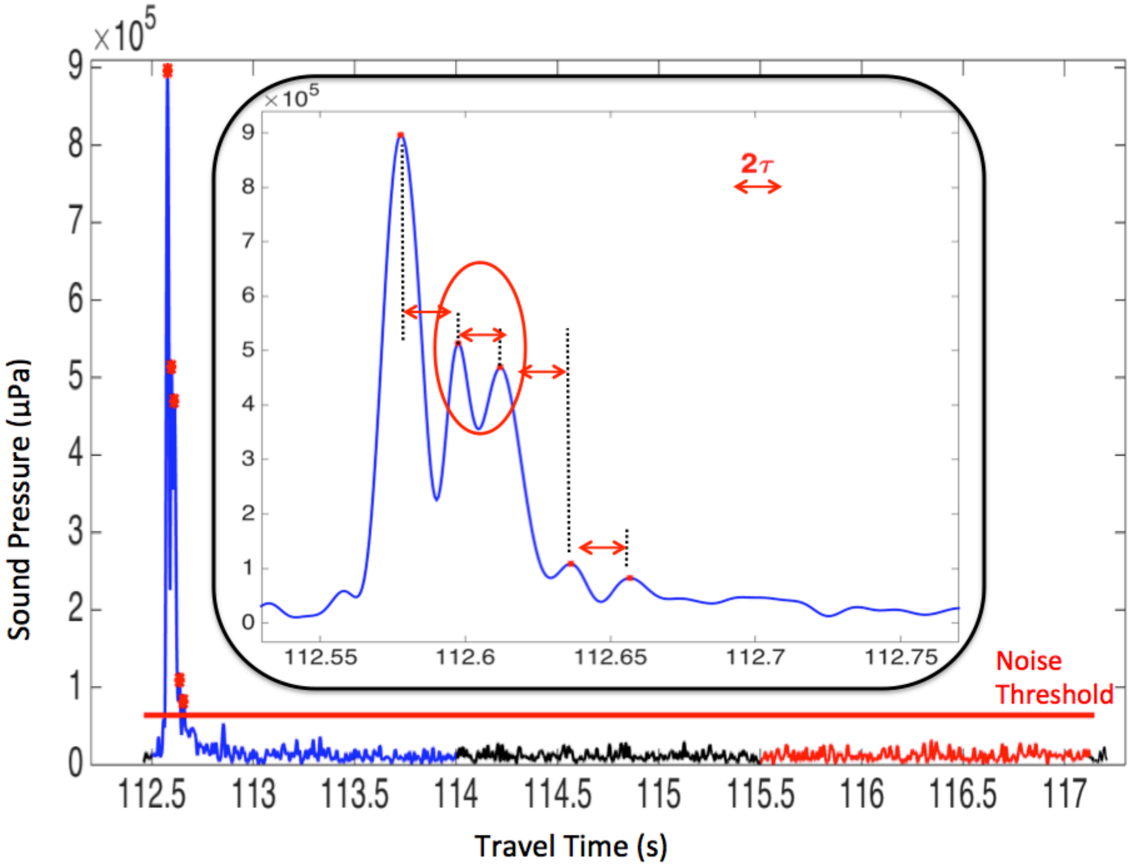

Figure 7. The signal (blue) and noise (red) segments in an arrival structure. The horizontal red line is the noise threshold (maximum noise level + 6dB) used to ensure the significance of an arrival. The figure inset shows the five significant arrivals (peaks marked as red dots). The red double arrows provide the 2τ minimum temporal separation distance for independent arrival determination. The temporal separation of the 2^{nd} and 3^{rd} arrivals fail to meet the "independence" criteria as their separation is less than less than 2τ, so they are counted as a single independent arrival. The 1^{st}, 4^{th}, and 5^{th} arrivals are independent, for a total of four arrivals.

III. RESULTS

A. SPECTRUM ANALYSIS

The spectral content of the temperature, travel times, and intensity were examined and integrated over three unique bands: the mesoscale (<0.5 cpd), internal tide (0.5~6.5 cpd) and high frequency internal wave (>6.5 cpd) scale, to discern spectral peaks and calculate variances. Frequency smoothing was used to trade spectral resolution for statistical reliability as described in the previous chapter.

1. Temperature Data Spectra

When the internal waves propagate through the basin, they cause thermal depression and temperature fluctuations. The east and west mooring temperature sensors capture the internal waves' energy, and six high amplitude peaks are observed in the spectra in the internal tidal band (Figure 8). The diurnal (D) and semidiurnal (SD) internal tides are strong, with weaker higher frequency (3~6 cpd) internal tidal constituents present. The spectra show that the semidiurnal peak level is smaller to the west (left), while the higher frequency tidal constituents' peak levels increase to the west, suggesting that the semidiurnal wave spawns higher frequencies during propagation. The semidiurnal internal tide has much larger amplitudes than the diurnal in the east. Larger amplitude waves are more nonlinear and tend to steepen more as they propagate, becoming more unstable and subsequently form high frequency waves. The diurnal peak levels in the east and west spectra are nearly at the same level, further suggesting that the diurnal internal waves transfer less energy into higher frequencies.

The energy transition of the semidiurnal internal tide to the high frequencies is consistent with Li and Farmer's (2011) vertical isopycnal displacement observations and their modeled results. Their data showed that the semidiurnal wave was prominent in the east and weak in the west, with more high frequency waves observed in the west. Their model suggests that no NIWs were formed if only the diurnal internal tide was present in the east basin.

Linearly fitting the spectra over the internal waves' band (Figure 8, pink lines), excluding the diurnal and semidiurnal internal tides, the slopes -1.7 and -1.6 (west/east) were found to differ from the Garrett-Munk spectrum slope of -2 (Garrett and Munk 1972, 1975) This is not surprising as the SCS internal waves are large, nonlinear and directional, while the Garrett-Munk spectrum assumes linear, isotropic, small-amplitude internal waves. Comparing the variances (Figure 8, blue numbers) induced by different scales of ocean fluctuations, shows that the internal tides (IT) dominate the temperature variance in the east and west, while the mesoscale (Meso), high frequency internal waves (HIW) have less effect on the temperature fluctuations.

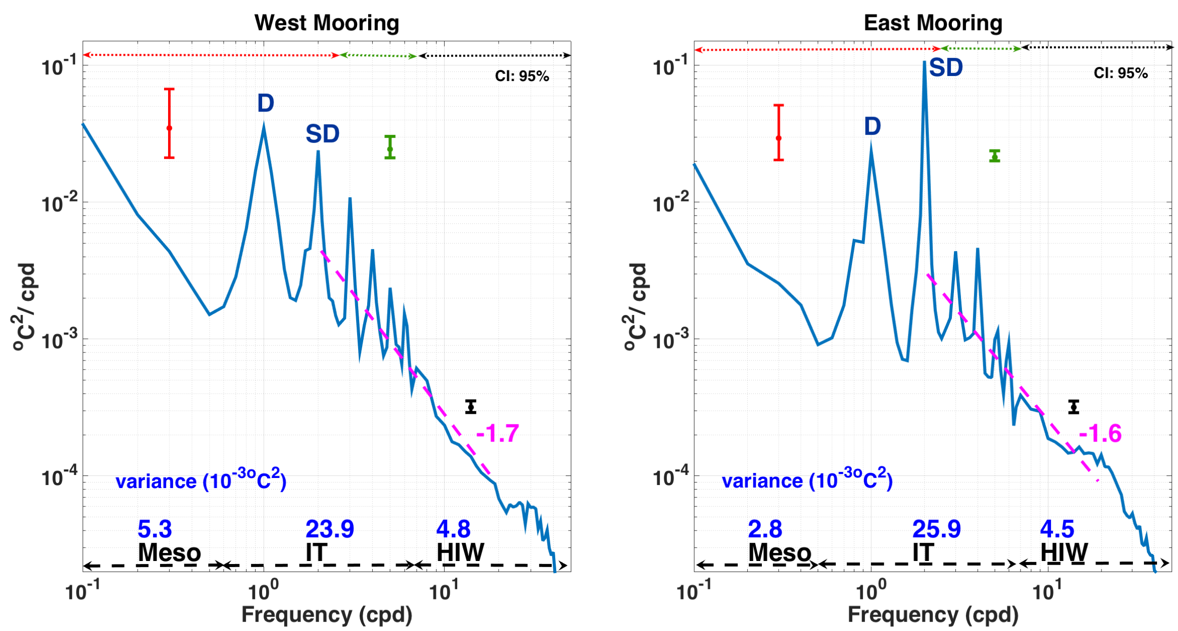

Figure 8. Temperature spectra observed at the west (left) and east (right) moorings over a four-month period. The vertical bars indicate the 95% confidence intervals, calculated for each of the frequency smoothing bands (red, green, black dashed lines at the top of each plot). Six internal tidal constituents are observed in both spectra, and the diurnal (D) and semidiurnal (SD) internal waves' energy are strong. The spectrum is integrated over the three frequency bands (black arrows) to calculate the mesoscale (Meso), internal tide (IT) and high frequency internal wave (HIW) variances (blue numbers). The magenta dashed lines show the first-degree polynomial fittings for the spectra over the internal wave band.

2. Signal Travel Times and Intensity Spectra

The signal travel-time and intensity spectra were estimated using the same methodology used to generate the temperature spectra, and the variances were calculated in terms of the mesoscale and internal tide, and high frequency internal wave scales.

The diurnal and semidiurnal internal tide signals are seen in the early-arrival travel time spectrum (left) and late-arrival (middle) spectra in Figure 9. One possible explanation for the lower diurnal and semidiurnal signatures in the late-arrival spectra is the late arrival ray paths span the entire water column, sampling the thermocline less frequently than the early arrival rays. As such, they are less influenced by the internal wave field, resulting in smaller diurnal and semidiurnal signatures. The higher frequency constituents seen in the temperature spectrum are not visible in the acoustic spectrum, because the small-scale spatial variability induced by the high frequency waves is much reduced in the path-averaged travel time measurement. The diurnal and semidiurnal tides also affect the signal intensity fluctuations, which can be seen in the spectrum (right). One possible explanation is the diurnal and semidiurnal waves depress the acoustic-signal ray paths, changing the bottom interactions and inducing signal intensity fluctuations.

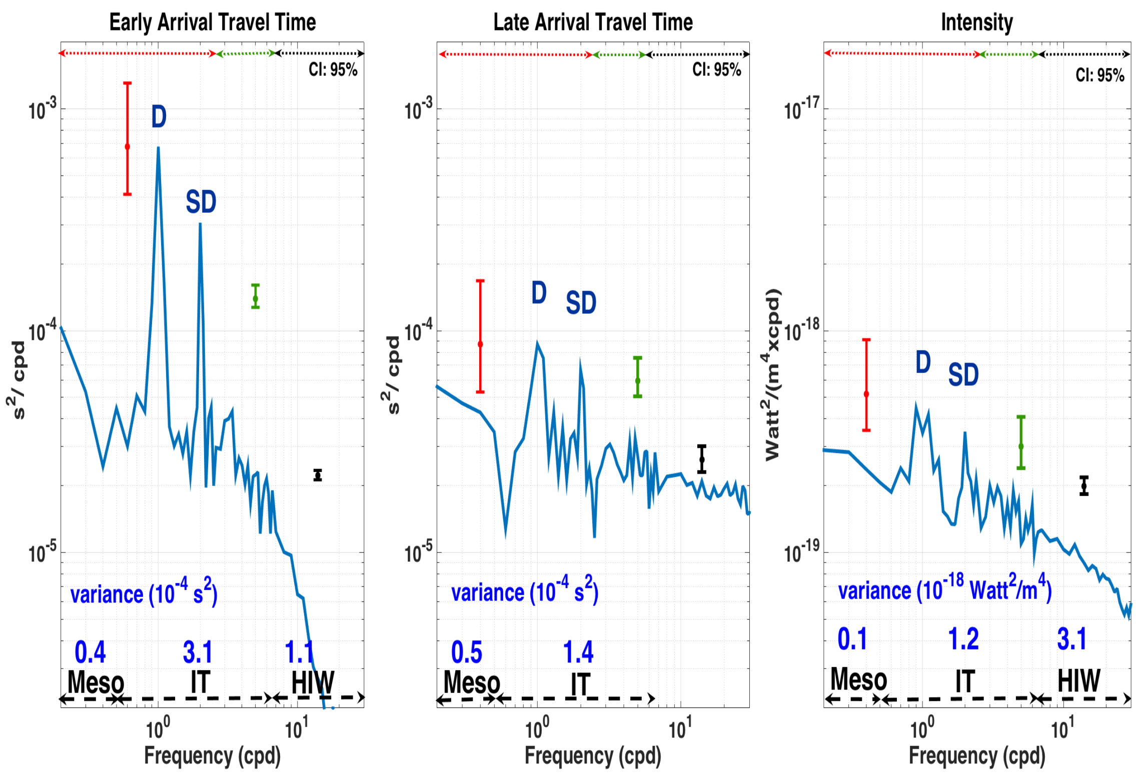

Figure 9. Travel time spectra of the early (left) and late (middle) arrival, and the signal intensity spectrum (right). The vertical bars indicate the 95% confidence intervals, calculated for each of the frequency smoothing bands (red, green, black dashed lines at the top of each plot). The diurnal (D) and semidiurnal (SD) internal tide constituents are clearly seen in all acoustic spectra. Mesoscale (Meso), internal tide (IT) and high frequency internal wave (HIW) bands used to calculate variance estimates (blue numbers) are shown. Flattening in the HIW band of the late arrival spectrum indicates random noise contamination, and has been excluded.

Comparing the variances (blue numbers, Figure 9) of the travel times and signal intensity, the travel time variances are dominated by the large spatial-scale internal tides, while the signal intensity variance is dominated by the small spatial-scale HIW fluctuations. Intensity fluctuation depends on the gradients of the sound speed profile. The high frequency waves create larger gradients, which causes more scattering, thus those waves induce more intensity variability than the low frequency waves. The late-arrival travel time variance in the HIW band had been excluded, because the flattened spectrum indicates random noise contamination in this band.

B. COHERENCE

The east and west temperature signals (Figure 10, top) show significant coherence at the semidiurnal frequency, and another coherence at a shifted diurnal frequency of ~1.3 cpd. One possible reason for the diurnal frequency shift is significant waveform change or distortion between these measurements, due to the rotational dispersion (Helfrich and Grimshaw, 2008).

Squared coherence of the early/late-arrival travel times compared to the east mooring temperature (Figure 10, middle), and west mooring temperature (Figure 10, bottom) were calculated. Strong semidiurnal coherence is observed between all data. The east mooring temperature shows no coherence to the early travel time arrival at the diurnal frequency, but the late arrival shows some coherence at a frequency lower than the diurnal tide. The west mooring temperature shows strong coherence to a slightly shifted diurnal frequency, suggesting that in the travel time variances in the tidal bands are more related to the temperature fluctuations in the west basin.

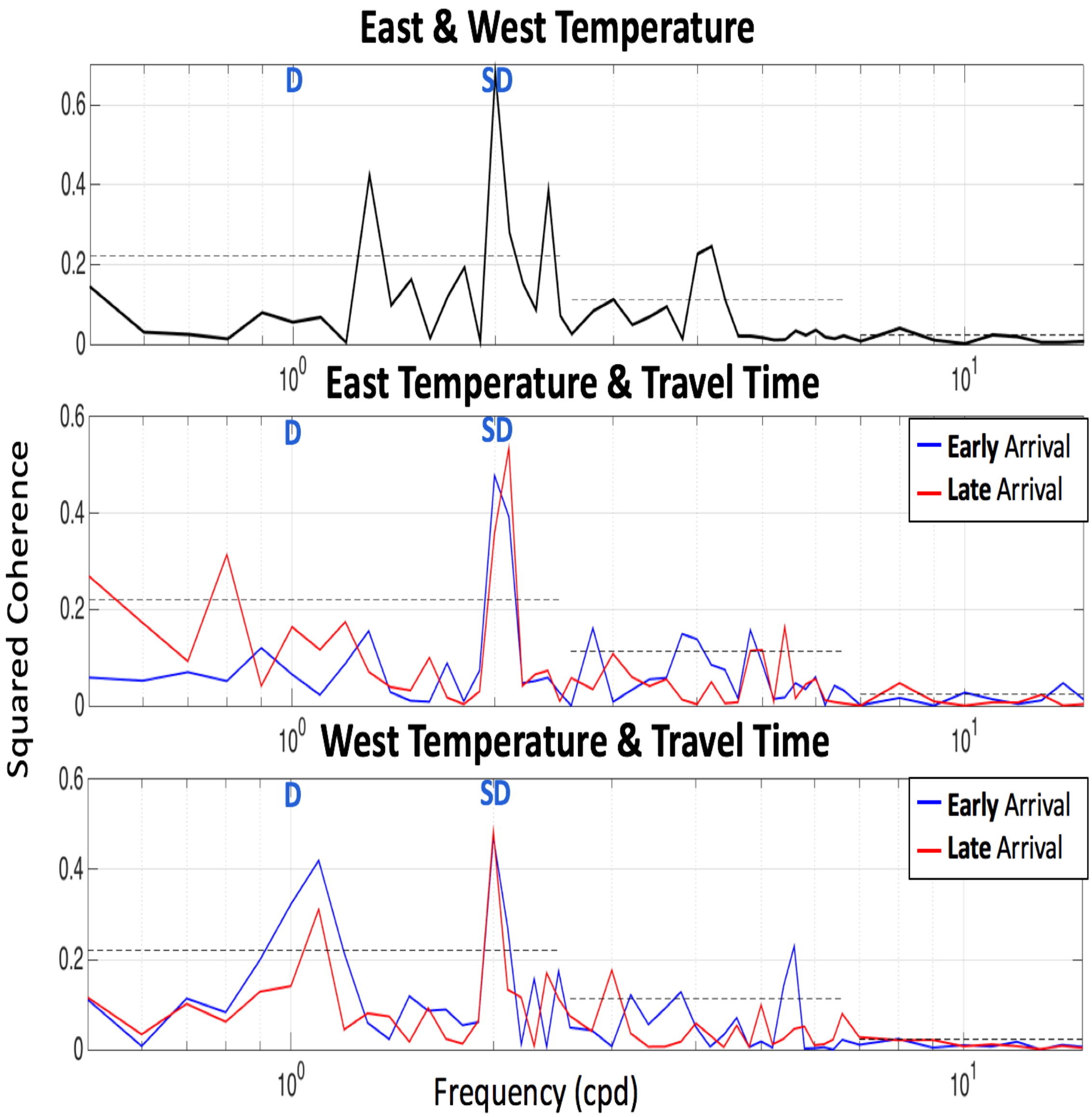

Figure 10. The square coherence spectra for east and west mooring temperature (top); east mooring temperature and early (blue) /late (red) arrival travel time (middle), west mooring temperature and early (blue) /late (red) arrival travel time (bottom). The dashed horizontal lines indicate the 95% pure chance limits. The east and west temperatures show significant coherence in the IT frequencies. The travel time in the semidiurnal IT frequency has a strong linear relationship with the west and east temperature.

C. RELATING THE INTENSITY LEVEL STATISTICS TO THE NUMBER OF INDEPENDENT ARRIVALS

Following the modified Dyer theory proposed by Reeves (2008), the sound intensity level and the number of arrivals of each transmission were estimated using the criteria discussed in Chapter II. Using multiple bandwidths and 6-hr, 12-hr, 1-day and 2-day ensemble lengths, statistics were calculated to study the applicability of this modified theory to deep-water propagation.

For each ensemble, the standard deviation of the SIL and the average number of arrivals were calculated, to compare with Dyer's 1970 theoretical curve (Figure 11). As the number of samples in the estimate of each statistics increases, the observations (colored dots) converge to the theoretical (black) curve.

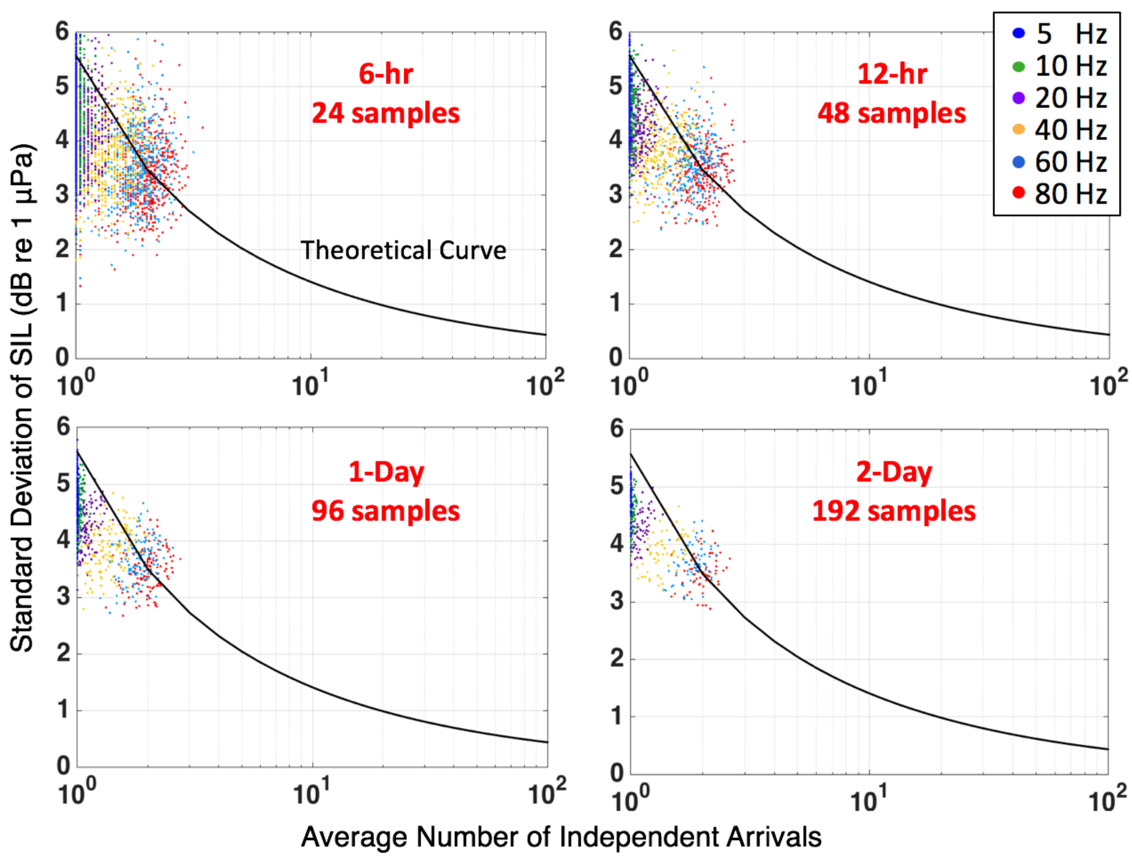

Figure 11. Standard deviation of the sound intensity level vs. average number of independent arrivals. The observations (dots) converge to the theoretical curve (black) as the ensemble length increases.

THIS PAGE INTENTIONALLY LEFT BLANK

IV. CONCLUSIONS

The conclusions of this study are summarized as follows:

- The temperature and travel time variances were dominated by the tidal band.
- The signal intensity variance was the largest in the high frequency internal wave band.
- The travel time variance in the tidal band was more related to the temperature fluctuations in the west of the basin.
- The SIL fluctuation was adequately predicted by the modified Dyer's theory.

THIS PAGE INTENTIONALLY LEFT BLANK

LIST OF REFERENCES

Bernotavicius, C.S., Chiu, C.-S., Miller, C.W., Reeder, D.B., Wei, R.-C.,Yang, Y.-J., and Chiu, L., "Modeling the basic arrival structure of a 400-Hz acoustic pulse through the South China Sea basin," *J. Comp. Acoust.*, **18**(2). 193–208 (2010).

Dyer, I., "Statistics of sound propagation in the ocean," *J. Acoust. Soc. Am.* **48**. 337–345 (1970).

Emery, W.J., and Thompson, R. E., *Data Analysis Methods in Physical Oceanography*. Elsevier, 451 pp (2004).

Garrett, C. J., Munk, W., "Space–time scales of internal waves," *Geophys. Fluid Dyn.,* **2,** 255–264 (1972).

Garrett, C. J., Munk, W., "Space–time scales of internal waves: A progress report," *J. Geophys. Res.,* **80,** 291–297. (1975)

Helfrich, K.R., and Grimshaw, R.H.J., Nonlinear disintegration of the internal tide. *J. Geophys. Res.*, **91**, 7697–7708 (2008).

Li, Q. & Farmer, D. "The generation and evolution of nonlinear internal waves in the deep basin of the South China Sea." *J. Phys. Oceanogr.* **41**, 1345–1363 (2011).

Ramp, S. R., Yang, Y. J., and Bahr, F. L., " Characterizing the nonlinear internal wave climate in the northeastern South China Sea," *Nonlin. Processes Geophys.*, **17**, 481–498, doi:10.5194/n pg-17-481 (2010).

Reeves, J.M., "Statistics of acoustic pulse signals through nonlinear internal waves on the continental shelf of the Northeastern South China Sea," Dissertation, Naval Postgraduate School, 2008.

Thompson, R. O. R. Y., Coherence Significance Levels, *J. Atmos. Sci.*, **36**, 2020–2021 (1979).

THIS PAGE INTENTIONALLY LEFT BLANK

INITIAL DISTRIBUTION LIST

1. Defense Technical Information Center
   Ft. Belvoir, Virginia

2. Dudley Knox Library
   Naval Postgraduate School
   Monterey, California